LA-UR-04-8337

Approved for public release;
distribution is unlimited.

Title:	TUFF FRACTURE CHARACTERIZATION ALONG MORTANDAD CANYON BETWEEN OU-1114 AND OU-1129
Authors:	Kenneth H. Wohletz, EES-11
Submitted to:	LANL ER Project

Form 836 (8/00)

Tuff Fracture Characterization Along Mortandad Canyon Between OU-1114 And OU-1129

Kenneth H. Wohletz

Los Alamos National Laboratory

ABSTRACT

Documentation of 2296 fractures in the Bandelier Tuff in the upper reaches of Mortandad Canyon between OU-1114 and OU-1129 characterizes features that can be related to the cooling history of the tuff, their subsequent tectonic deformation, and their potential affects on contaminant migration in the Canyon. Fractures were characterized in unit 3 of the Tshirege Member along a section beginning at E484200 on the state plane grid and running nearly 6100 feet to the east. Fractures show conjugate sets with mean strikes at N22W and N82E, a third minor set strikes near N50W. These fractures are steeply dipping and owe their primary orientation to contraction of tuff as it cooled in the months to years after it was emplaced. The conjugate nature of fracture orientations indicates a principal horizontal stress field oriented approximately N15E, but deformation during cooling compaction of the tuff over the shoulder of the pre-Bandelier Mortandad canyon wall has resulted in a dominance of nearly E-W-trending fractures. Linear fracture density rises from a background of approximately 20 to over 100 and 60 fractures per hundred feet over the trace of the Rendija Canyon (RCF) and Guaje Mountain (GMF) faults, respectively. These traces are roughly N-S oriented, and as a result of this study, are mapped at E484278 (RCF) and E487288 (GMF). Increased fracture density and aperture as well as increased variability in fracture strike and dip occur over ranges of 600 and 2000 feet centered over the RCF and GMF, respectively. The variation in fracture characteristics can be explained in part by assuming tectonic deformation was accommodated by in these fractures. Assuming that the deformation produced normal faults with west sides down, the variations in fracture density, strike, dip, and aperture can be calculated to show 11.3 and 3.7 m down-to-the-west over the RCF and GMF, respectively. This result can only have been calculated if there is some non-random progression in fracture characteristics along the measured section. The overall result of this study then suggests that water movement down Mortandad Canyon may likely be influenced where it crosses these faults. The influence, if any, would be a pathway for surface runoff to infiltrate downward into bedrock, perhaps reaching a perched aquifer below and an alluvial aquifer in lower reaches of the canyon.

INTRODUCTION

The Tshirege (upper) Member of the Bandelier Tuff contains numerous rock fractures throughout its total areal extent, including areas underlying Los Alamos National Laboratory. These fractures are geologically termed *joints* and are a common feature of welded ash-flow tuffs, such as the Bandelier Tuff. These fractures are an important and very obvious physical feature of the tuff and play an important role in appraisal of geological characteristics that might affect environmental remediation studies (Purtymun and Kennedy, 1971; Purtymun et al. 1978). First of all, following previous studies of fractured tuff by Barton and Hsieh (1989) and Fuller and Sharp (1992), their presence and abundance are key factors in understanding the vadose-zone hydrology and their possible effect on contaminant infiltration from waste disposal areas. In addition, the fractures show characteristics that can help determine tectonic movement along faults crossing the Pajarito Plateau (Vaniman and Wohletz, 1990).

Recently, studies of these fractures were undertaken to evaluate their relationship to tectonic fault zones, the Rendija Canyon Fault (RCF) and the Guaje Mountain Fault (GMF), underlying the laboratory areas and the possible seismic hazard to laboratory structures (Vaniman and Wohletz, 1990). This present study builds on that earlier work and complementary work by Walters (1996) and Wohletz (1995; 1996).

This study concerns fractures exposed in unit 3 of the Bandelier Tuff in Mortandad Canyon. The study documents fractures in a measured section, starting at a point about 4800 feet east of Diamond Drive (N1771400 and E484200 on the New Mexico State Plane), spanning nearly 6100 feet east along the north wall of Mortandad Canyon, parallel to the boundary between Operational Units OU-1114 to the north and OU-1129 to the south. Unit 3 of the Tshirege Member forms a continuous cliff along the canyon below Sigma Mesa and unit 2 forms an inner-canyon cliff just north of TA-35 (see Fig. 1). Initial field work began during the summer of 1995 and was completed in August 1998. Following the methodology outlined below, the present fracture traverse comprises eleven photomosaic maps, constructed to document fractures in unit 3 along the canyon (Fig. 1). All locations discussed will be in feet east of the west end of the fracture traverse.

METHODOLOGY

The methodology follows three phases of study outlined by the *ER Fracture Characterization SOP* (LANL-ER-SOP-03.06): (1) photographic documentation of area or traverse along which fractures will be characterized, with construction of a photomosaic map base; (2) measurement and plotting of fracture geometry on the photomosaic map; and (3) statistical analysis of fracture data by procedures described below.

Photo Documentation. In photographing unit 3 of the Tshirege Member, successive stations at the base of the unit where slopes are accessible were set up such that focal distances of about 40 to 60 feet were maintained and photographs had about 20% overlap. Due to the curvature of the cliff face and its irregular vertical extent, each photograph covered and average between 30 to 50 feet of lateral exposure; scales added to the photomosaics reflect this variable lateral scale. After construction of the photomosaic, it was scanned into an electronic image from which a line drawing overlay was constructed. This overlay provided a base map of outcrop features including key topographic points such as cliff tops and bottoms, prominent fractures, and geographic objects such as buildings, trees, and large sign posts. This map was attached to the base of the photomosaic such that a one-to-one correspondence can be made between mapped and photographed features. The 6059 foot traverse required 14 individual photomosaic maps. Figure 2 is an example of the fracture mosaic maps for the section of cliff exposure midway along the section.

Fracture Measurement. The horizontal scale for the fracture maps was determined by measuring distance on the topographic map between topographic points identified on the photomosaics. Because FIMAD maps use the foot scale for positional data, this scale is retained; however, in this study, the metric system is used for fracture aperture and displacements, because

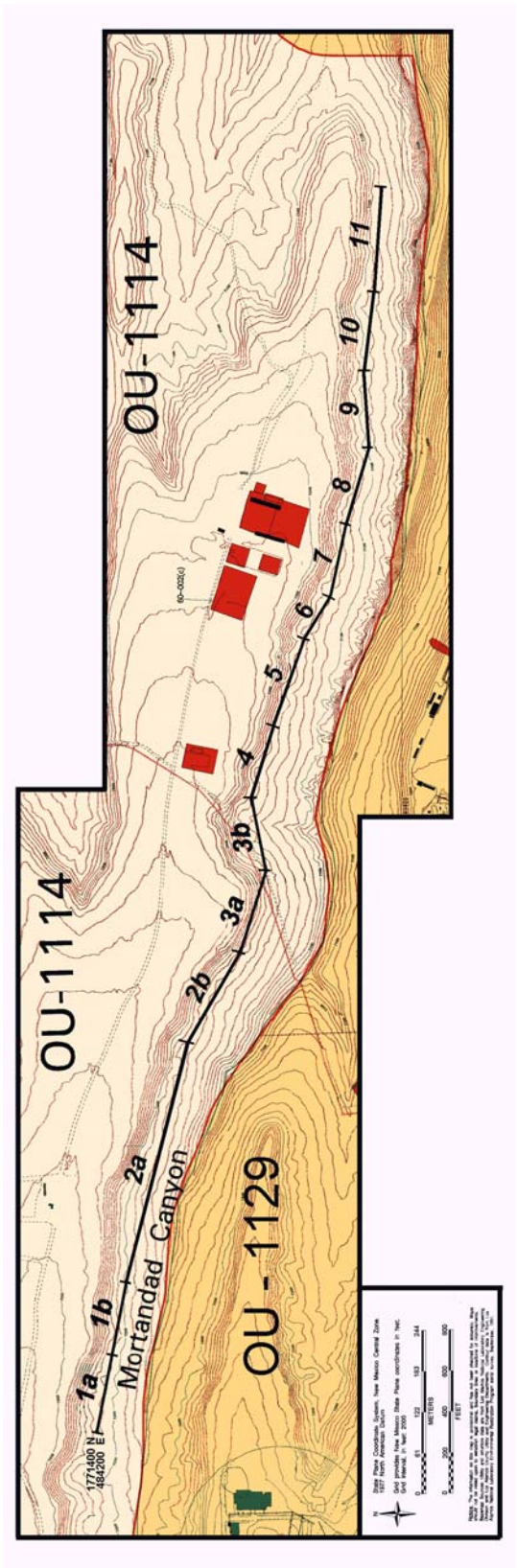

Fig. 1: Location map for the fracture characterization traverse along Mortandad Canyon. Numbered segments refer to specific fracture maps created and are used to orient plots in this paper.

it facilitates fracture calculations. The horizontal scale was then placed upon the map to show the distance between mapped features. Because of topographic irregularities of the cliff face described above, this scale will have an error of about ±10% of each map's total width. Starting from one end of the fracture traverse, each fracture was sketched upon the map and designated by a number. These numbers increase from west to east and are pertinent only to the photomosaic map on which they are shown (e.g., fracture numbers 1 through 129 of Mortandad Section 4, Fig. 2). Because fracture exposure and accessibility are not ideal for precise measurement, fracture measurements have intrinsic errors of approximately 10 feet in location (at their average point of intersection with the map), 5 degrees in strike and dip (Brunton compass measurement), and 0.5 cm in aperture (measured perpendicular to fracture surfaces). These errors, however, are similar to the natural variability in individual fracture character (demonstrated on photomosaic maps), each fracture being sinuous and of variable strike, dip, and aperture. In cases where fractures could not be safely accessed, standard Brunton compass techniques were applied, which require measurement using the compass alignment sights with cautious observation of the relationship between true and apparent orientations. All observed fractures have been recorded with some parallel sets too closely spaced to be given individual numbers on the maps, but nonetheless they were recorded in the field notebook.

Fracture Data Base and Analysis. The fracture data, recorded in the field notebook, were entered into an computer data base, which allowed application of several statistical procedures. The data base consists of a table with a column for each fracture listing the fracture's number designation, its horizontal location shown on the fracture map, its dip and strike, and its aperture. From these data several other columns are statistically calculated, including: (1) a linear fracture density calculated as a moving average by counting the number of fractures contained in a given distance interval (10 and 100 feet) centered on each fracture; (2) a cumulative fracture aperture over a specified interval (100 feet) centered on each fracture; (3) relative dip of fracture from vertical where negative values indicate southerly inclinations; and (4) fracture vertical displacement, both individual and cumulative. Because these fractures have their initial origin as cooling joints and cross-cutting relationships suggest that these two groups are coeval, a conjugate joint set is expected to be displayed by grouping of fracture strike orientations separated by 60 to 90 degrees of azimuth with average trends in the NW-SE and NE-SW quadrants. For purposes of analysis, fractures are grouped according to their strike of NW or NE.

Additionally, fractures have dip plunges toward the south and north, which serves as a secondary means of analysis. Accordingly, additional columns for the table are separately calculated for fracture density and cumulative fracture aperture for each strike and dip set. Numerical procedures for the above calculations are: (1) calculation of linear fracture densities for several different distance intervals, taking into account section end effects by extrapolation of the gradient of density with distance; (2) transformation of azimuth and dip measurements to strikes and dips as degrees from vertical, respectively; (3) computation of cumulative fracture widths for 10 and 100 foot distance intervals; and (4) calculation of apparent fracture vertical displacement. While more sophisticated statistical analyses can be applied to these data sets, those used are sufficient to characterize the fractures.

Fracture data were then displayed on several different plots using a LOWESS (Locally Weighted Regression Scatter Plot Smoothing) algorithm to better illustrate data trends. A weighting factor of 0.1 was chosen, which represents a smoothing over approximately 230 adjacent points. The plots consists of (1) fracture density (100 foot intervals) *vs* horizontal distance along the traverse; (2) rose and stereonet diagrams of fracture strike; (3) fracture strike *vs* horizontal distance where positive strikes represent strike in degrees east of north and negative strikes are west of north; (4) fracture dips *vs* horizontal distance where vertical plots at zero, dips

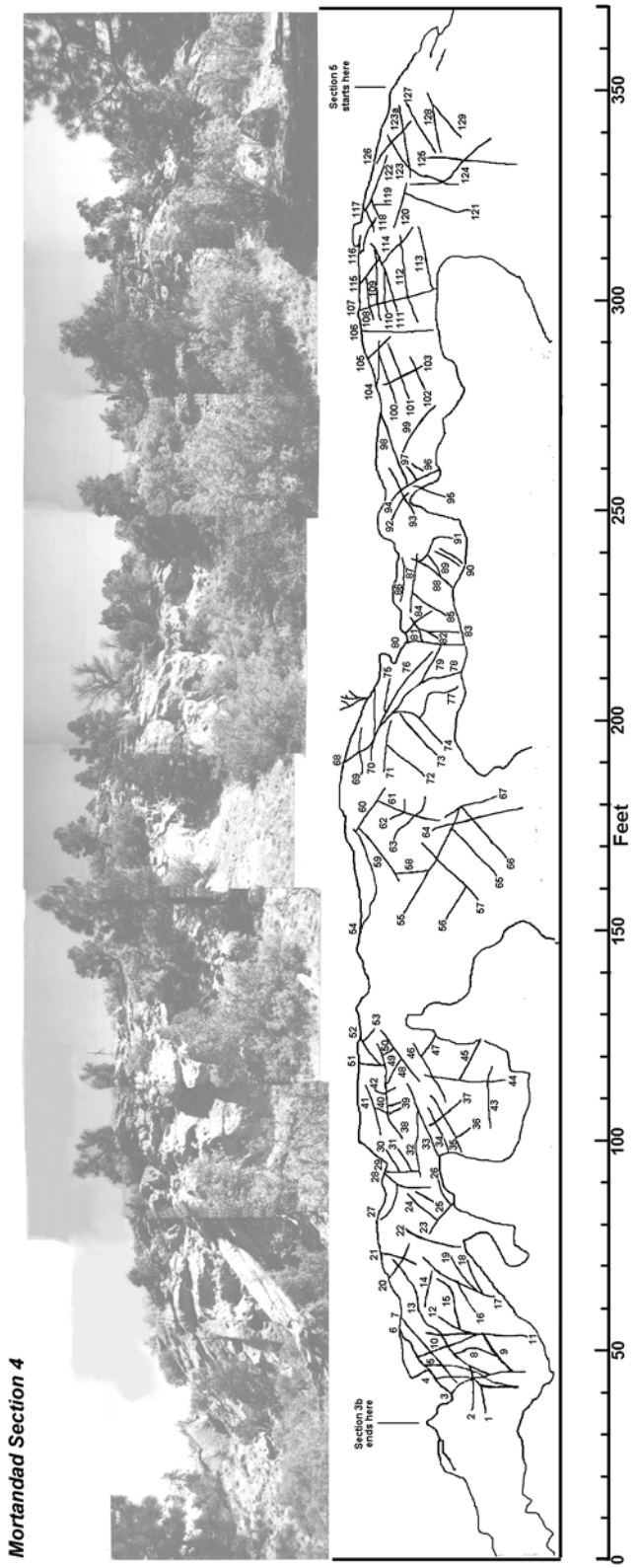

Fig. 2: Example photomosaic and fracture map of Mortandad section 4, located just east of the pipe-line access road into Mortandad Canyon from Sigma Mesa. Each documented fracture has a number for its identification in the fracture data base.

toward the northeast or northwest are positive inflections from vertical, and southerly dips are negative inflections from vertical; (5) fracture apertures and cumulative fracture widths (per 100 foot interval) *vs* horizontal distance; and (6) apparent vertical displacement per 100-foot interval and cumulatively over the entire section. These plots can show anomalous fracture characteristics in areas of a fault zone (Vaniman and Wohletz, 1990).

FRACTURE CHARACTER

A total of 2296 fractures were documented in the 6059 feet along the north side of Mortandad Canyon adjacent to Sigma Mesa. The character of these fractures has much in common with that discussed by Vaniman and Wohletz (1990) and Wohletz (1995, 1996), and the reader is encouraged to compare these data with those of earlier reports for other areas. The characteristics discussed are fracture linear density, strike, dip, and aperture. In describing these data, statistical values are shown for all fractures and for individual strike/dip sets.

Fracture Density. Linear fracture density data is listed in Table 1 and portrayed in Figure 3 as the number of fractures within a 10- and 100-foot interval centered on each fracture for the Mortandad section. Table 1 shows a mean value of 42 fractures per 100-foot interval with the NE-striking and northerly dipping sets slightly more abundant than the NW-striking and southerly dipping sets.

The variation of fracture density per 100-foot intervals with distance along the measured section shows peaks reaching 100 fractures per 100 feet and 60 fractures per 100 feet over parts of the section crossing what are likely traces of the Rendija Canyon and Guaje Mountain faults, respectively. Between these two fault zones and to the east of the latter, fracture densities fall off to about 20 fractures per 100-foot interval, which represents a background average for fracture density in laboratory areas as found in previous studies by Vaniman and Wohletz (1990) and Wohletz (1995, 1996).

Figures 4 and 5 show smoothed fracture densities for NW- and NE-striking and N- and S-dipping fracture sets compared to that for all fractures, respectively. Note that NE-striking and N-dipping fractures have greater density that do NW-striking and S-dipping fractures. This

character comes from the fact that NE-striking and N-dipping fractures are the most common types. While the trend in density is similar for both strike sets, the dip sets show more abundant S-dipping fractures from 200 to 1100 feet east (RCF) and that N-dipping fractures show much greater density variation than S-dipping ones from 2500 to 4500 east (GMF).

Table 1. Fracture Density Data for Mortandad Canyon

Fracture Set	*Number*	*Mean (#/100 ft)*	*Standard Deviation*
All	2296	42	±19
NW	702	14	±6
NE	1090	22	±11
N	1541	30	±11
S	755	16	±13

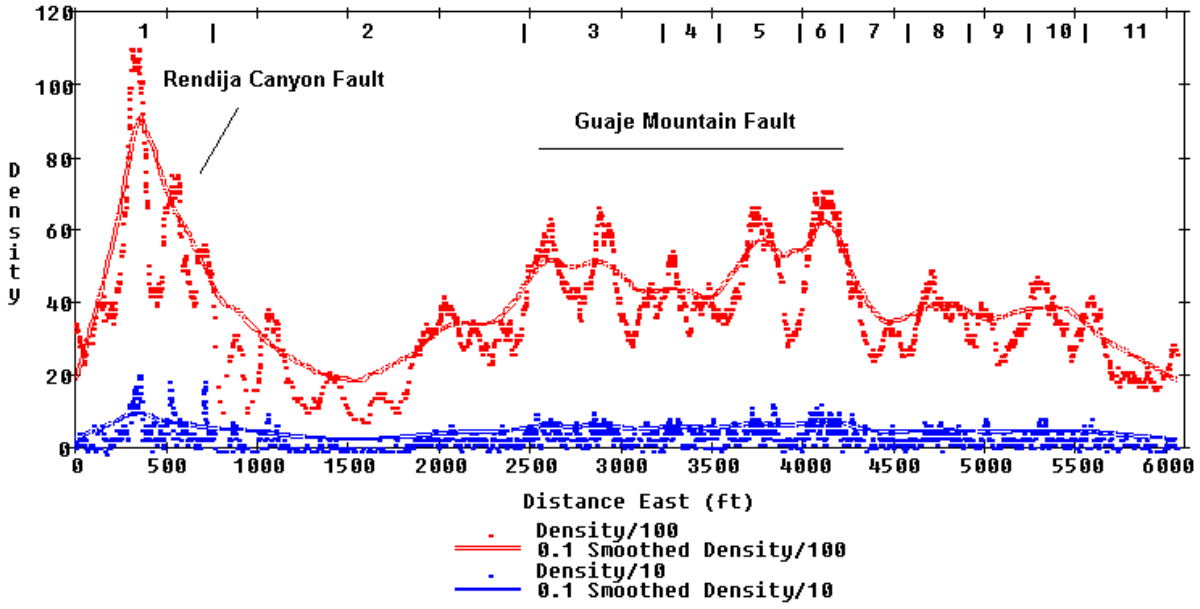

Fig. 3: Fracture density shows the number of fractures per 10 and 100-foot intervals centered on each fracture along the traverse of approximately 6100 feet. The density/10-foot interval curve depicts the visual impression one may obtain from field inspection, but the density/100-foot interval curve shows very apparent peaks in fracture density over a rang from about 250 to 750 feet east and from 2500 to 4250 feet east. These peaks are thought to correspond the Rendija Canyon Fault and Guaje Mountain Fault zones, respectively.

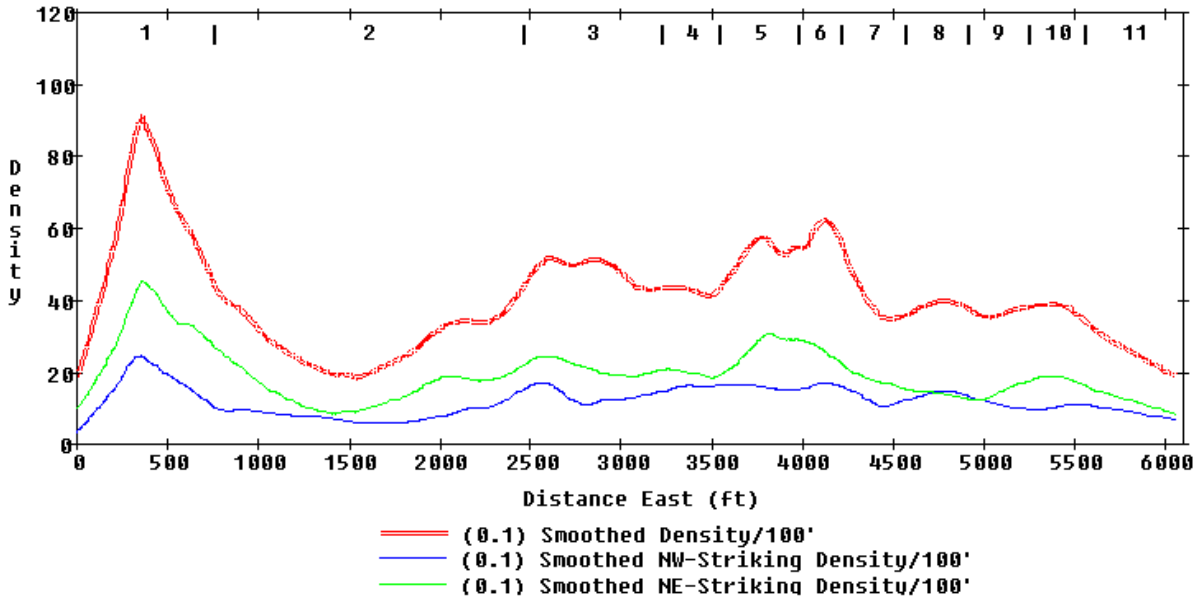

Fig. 4: Variation of fracture density per 100-foot interval for all fractures and for those belonging to the NW- and NE-striking sets.

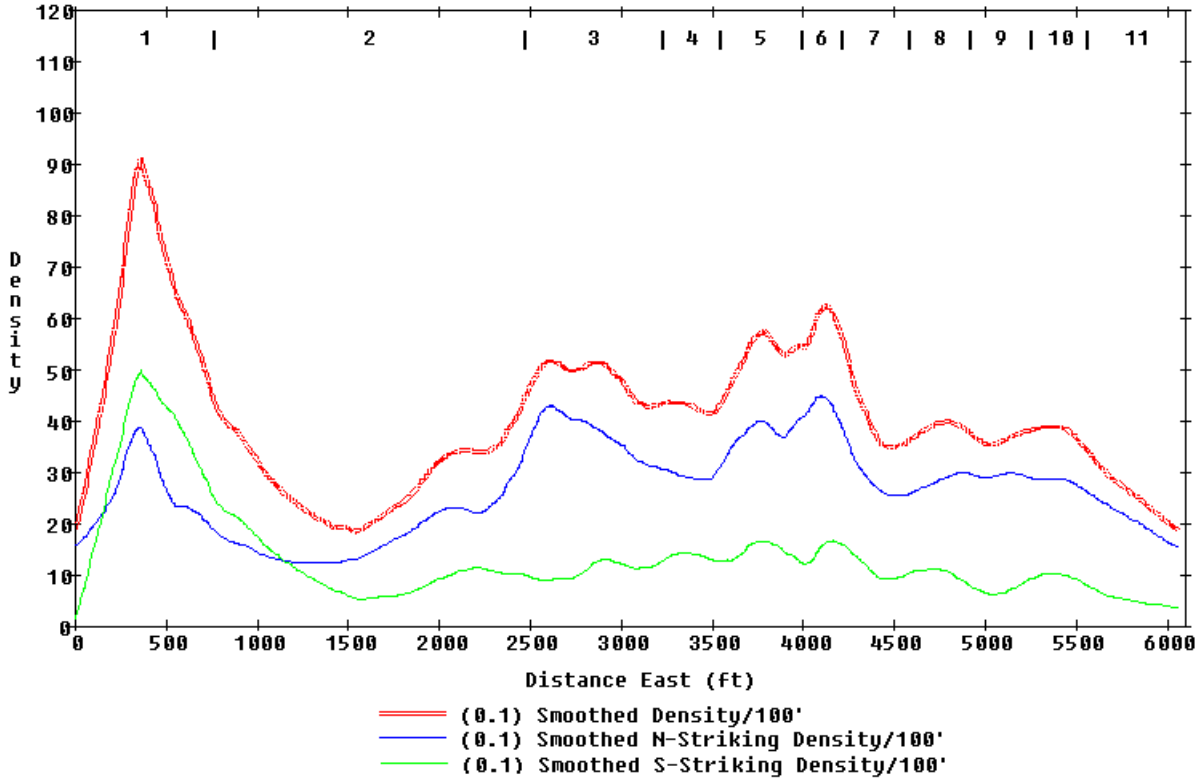

Fig. 5: Variation of fracture density per 100-foot interval for all fractures and for those belonging to the N- and S-dipping sets.

Fracture Strike. Plotted in a rose diagram (Fig. 6), fracture strikes show two groupings with mean strikes: a major mode at N82E (NE set) and a minor one at N22W (NW set), supporting the conjugate joint-set assumption for distribution of the fractures. It is possible that the NE set has some contribution by E-W fractures, formed as a results of flexure of the tuff over paleotopography running E-W along an ancestral Mortandad Canyon, as discussed by Wohletz (1966).

Table 2 shows the statistical variation in fracture strikes. The mean strike in nearly E-W, and this is true for both N- and S-dipping fractures, but the standard deviation of ±51° indicates quite a spread in this data. The NW set of fractures (N26W ±14°) comprise those with strikes in the range of N50W to N0W (Fig. 6), while the NE set (N80E ±22°) is broader and encompasses fractures striking from N40E to and azimuth of 120°.

Figures 7 and 8 depict fracture strike variation along the canyon for all fractures and for the NE- and NW-striking and N- and S-dipping fracture sets. Note that strikes are shown as azimuths such that the NW-striking set has an azimuth varying around 160°. Because NE-striking fractures are most abundant, their smoothed curve plots close to that representing all fractures, nearly in E-W orientation. Both the curves for the NW and NE sets closely follow the trend for all fractures, with notable inflections occuring in ranges from 200 to 700 feet east and 2400 to 3700 feet east. I note that the NE set shows variations antithetic to those of all fractures in the latter range. This behavior likely reflects the nature of the GMF. The N- and S-dipping fracture sets show antithetic variations over these two ranges and over the range from 3700 to 5000 feet east. S-dipping fractures average in strike up to 30° more southerly than do N-dipping fractures that more closely match the strike of all fractures.

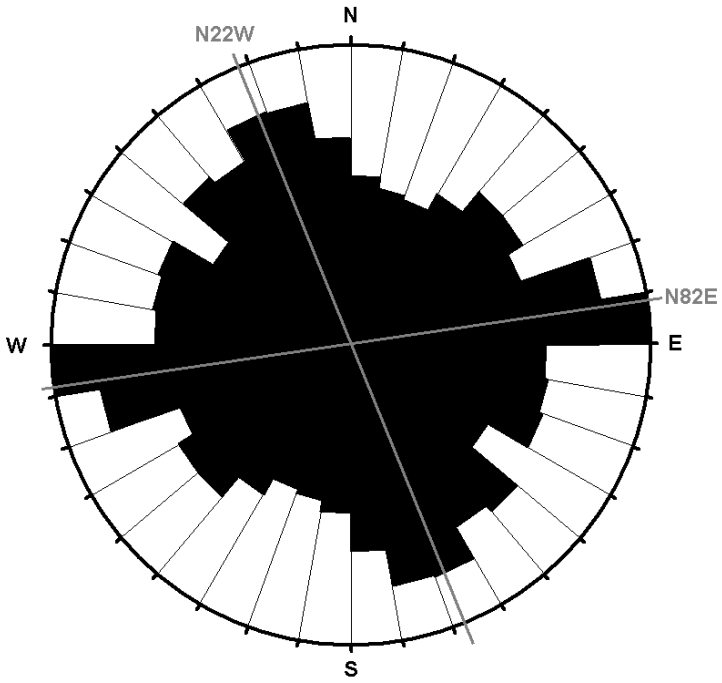

Fig. 6: A rose diagram of fracture strikes measured in Mortandad Canyon shows a preferred orientation in two directions, a NW set at N22W and a NE set at N82E.

Table 2. Fracture Strike Data for Mortandad Canyon

Fracture Set	*Number*	*Mean (°)*	*Standard Deviation (°)*
All	2296	N86W	±51
NW	702	N26W	±14
NE	1090	N80E	±22
N	1541	N89W	±50
S	755	N88W	±52

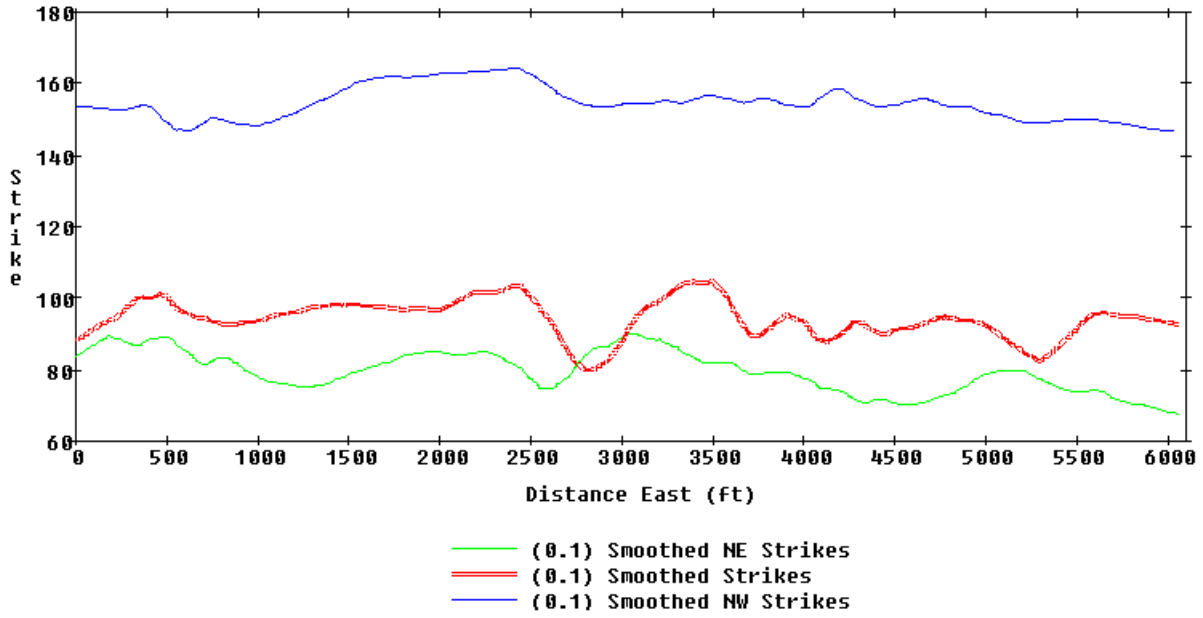

Fig. 7: Variation of smoothed fracture strikes(shown as azimuths) along the Mortandad Canyon traverse shows the average of all strikes and the average for those within the NW and NE sets.

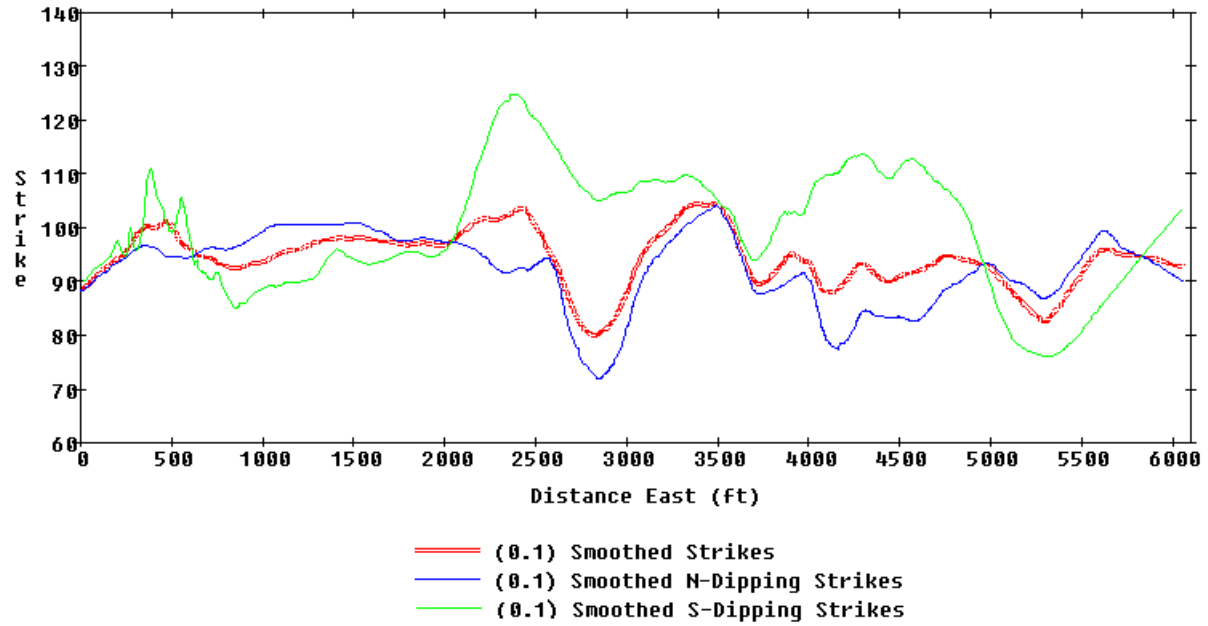

Fig. 8: Variation of smoothed fracture strikes (shown as azimuths) along the Mortandad Canyon traverse shows the average of all strikes and the average for those within the N- and S-dipping sets.

Fracture Dip. Fractures generally dip steeply (Table 3), with mean values near 84°N (from horizontal), attesting that northerly dipping fractures are over twice as abundant than southerly dipping ones. The standard deviation of ±38° for all fractures means that 95% of all fracture have a dip from 46°N to 58°S. NW-trending fractures are nearly vertical with steep inclines averaging to the south, while NE-trending fractures are not as steep and dip mostly to the north. Also northerly dipping fractures are somewhat steeper than southerly dipping ones.

One can define a fracture plunge as azimuth perpendicular to the strike in the direction of the dip (surveying definition). Plotting these plunges and their dips on the lower hemisphere of an equal area stereonet (Fig. 9) defines the poles for fractures (normals to the fracture plane). These poles define groupings showing two main fracture sets: a set of steeply dipping fractures (near the circumference of the stereonet) showing mostly NE strikes with both dips to north (southern hemisphere) and to the south (northern hemisphere); and a set of gently to moderately inclined fractures (central portion of the stereonet) dominantly represented by eastern strikes with northern dips (southern hemisphere grouping) and northwestern strikes with mostly southern dips (cluster in northeastern quadrant) and few northern dips (cluster in southwestern quadrant).

Figures 10 and 11 display the smoothed variation of fracture dips with distance for all fractures, for the NE- and NW-striking sets, and for the N- and S-dipping sets. In general fracture dips become more variable but less steeply dipping over areas where faults are proposed, that is from 250 to 750 feet east (RCF) and from 2500 to 4000 feet east (GMF).

Table 3. Fracture Dip Data for Mortandad Canyon

Fracture Set	*Number*	*Mean (°)*	*Standard Deviation (°)*
All	2296	84N	±38
NW	702	88S	±38
NE	1090	76N	±41
N	1541	63N	±26
S	755	55S	±24

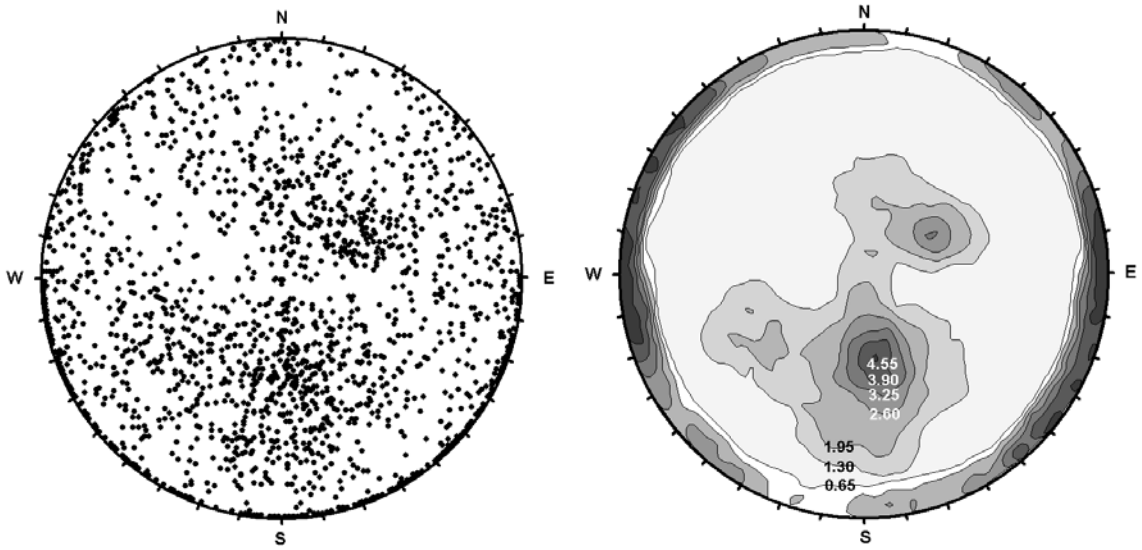

Fig. 9: Lower hemisphere, equal area plots of fracture poles show clustering dominated by nearly vertical NE-striking fractures and subordinated by gently to moderately dipping fractures of the easterly and northwesterly striking fractures. Numbers on the contours designate the percentage of fractures enclosed by the contour.

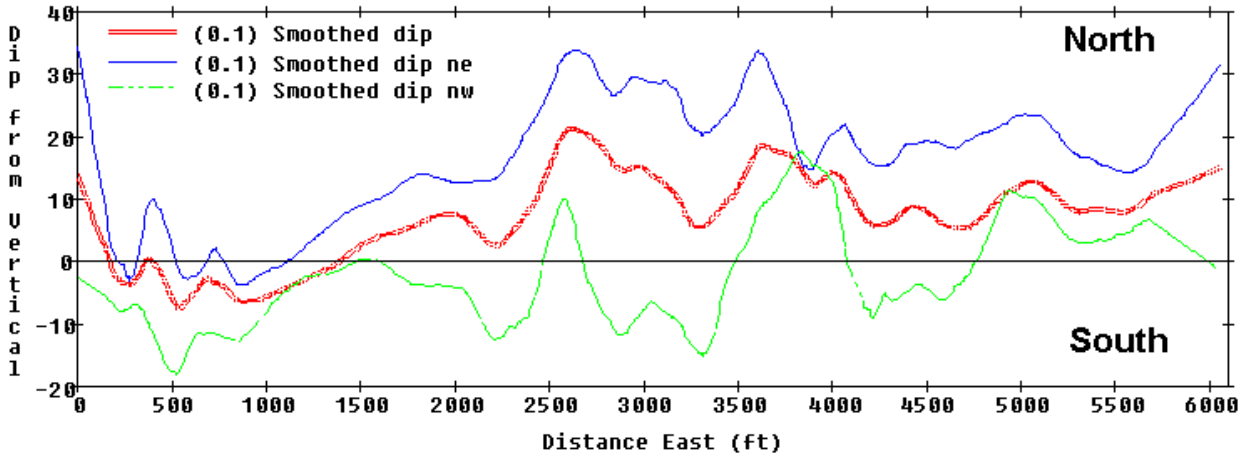

Fig. 10: Variation of fracture dips with distance, showing the smoothed variation for all dips and those for fractures belonging to the NE- and NW-striking fracture sets.

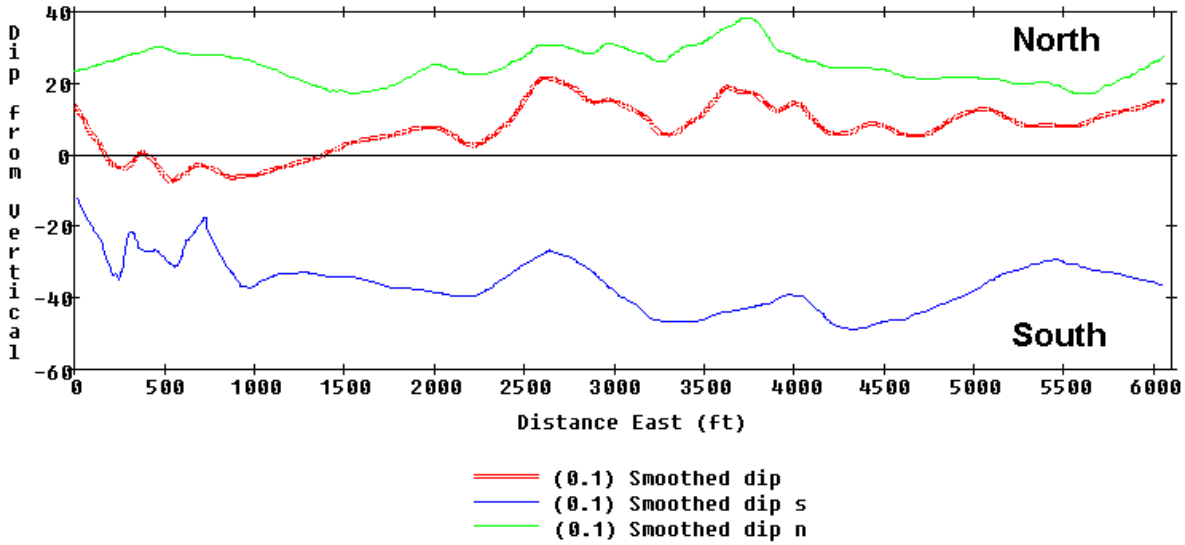

Fig. 11: Variation of fracture dips with distance, showing the smoothed variation for all dips and those for fractures belonging to the N- and S-dipping fracture sets.

Fracture Aperture. The mean fracture aperture is 0.8 cm (Table 4) with 95% of all fractures having from 0 to 1.9 cm of aperture. The mean value represents the average opening along the sinuous fractures that in places may be nearly closed and other places open. In unit 3, fracture filling materials (clastic detritus and authigenic minerals) were common in fractures where they were within 10 m of the mesa surface, but below this depth fracture fillings were

generally absent. While NW- and NE-striking fractures show the same mean aperture, S-dipping fractures showed slightly wider apertures than N-dipping fractures. Figures 12 and 13 show that apertures are widest over the RCF from 250 to 1000 feet east, and they generally decrease eastward, ranging between 0.4 and 0.6 cm over the GMF from 2500 to 4000 feet east, and less than 0.4 from 4000 feet eastward. Figure 13 shows that over most of the measured section, S-dipping fractures are about 0.2 cm wider than N-dipping ones, reaching 1.3 cm of aperture over the RCF; however, these fracture sets show the same aperture over the GMF between 2700 and 3600 feet east.

Table 4. Fracture Aperture Data for Mortandad Canyon

Fracture Set	*Number*	*Mean Aperture (cm)*	*Standard Deviation*
All	2296	0.8	+1.1/-0.8
NW	702	0.7	+1.0/-0.7
NE	1090	0.7	+1.1/-0.7
N	1541	0.7	+1.0/-0.7
S	755	0.9	+1.3/-0.9

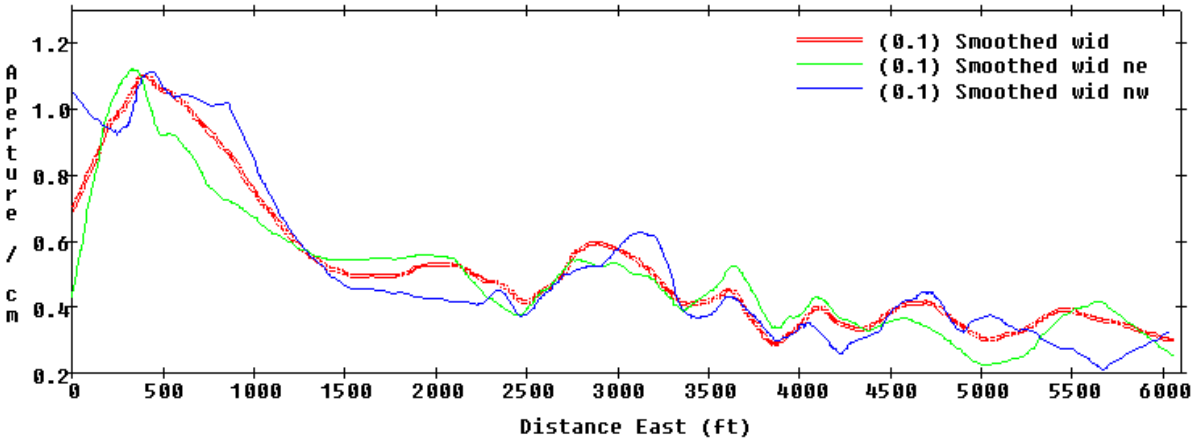

Fig. 12: Variation of fracture apertures with distance, showing the smoothed variation for all apertures and those for fractures belonging to the NE- and NW-striking fracture sets.

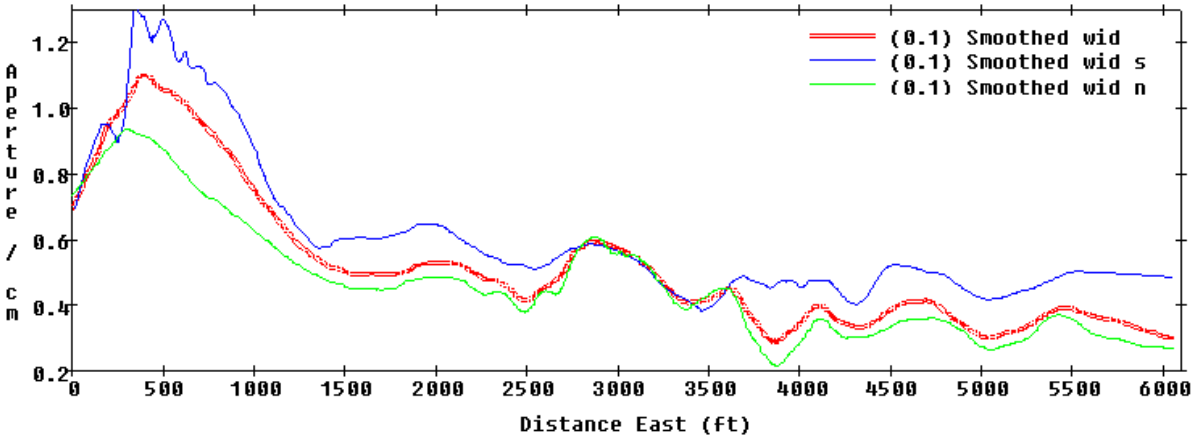

Fig. 13: Variation of fracture apertures with distance, showing the smoothed variation for all apertures and those for fractures belonging to the N- and S-dipping fracture sets.

DISCUSSION

The data presented above indicate that observed fractures in the Tshirege Member in Mortandad Canyon have origins from both cooling contraction of the tuff after its emplacement and subsequent adjustment of the tuff to tectonic movement along the Rendija Canyon and Guaje Mountain Faults. Based on these data, the fault trace for the GMF shown on the geological map presented by Vaniman and Wohletz (1990) is supported, but the trace of the RCF must be moved eastward about 500 feet. Accordingly, the geological map of the central portion of Los Alamos National Laboratory is here revised, showing zones of intense fracture in Mortandad Canyon and the new trace of the RCF (Fig. 14) The following discussion presents some interpretations and conclusions regarding (1) fracture geometry; (2) fracture origins; and (3) hydrologic effects of fractures in the Bandelier Tuff.

Fracture Geometry. While DeGraff and Aydin (1993) show that cooling contraction fractures show spacing inversely proportional to cooling rates, the observed increase in Bandelier Tuff fracture density (decrease in spacing) over the RCF and GMF (Fig. 3) can also be explained by two tectonic interpretations: (1) tectonic displacement is accommodated by preexisting fractures and incrementally dispersed over a wide area. In these areas, the greater number of fractures derives from tectonic stresses opening new cracks along zones of weakness or incipient

fractures originally caused by cooling contraction; and (2) a tectonic fracture pattern overprints the preexisting cooling fractures. Both interpretations can be supported in that (1) it is difficult to find evidence of significant displacement along most fractures in the form of offset lithologies, but (2) there are common structural features along fault traces such as *micrograbens* and *zipper joints* that suggest downdrop of individual blocks of tuff in isolated areas near the top of unit 2 (Vaniman and Wohletz, 1990). A consideration, discussed by DeGraff and Aydin (1993), is that convective movement of fluids in fractures during cooling will increase the overall cooling rate resulting in more closely spaced fractures. In that light, one might also suppose that the increased fracture density areas represent areas of convective cooling in the tuff, but increased occurrences of fumarolic pipes and vapor-phase alteration, which result from such cooling, have not been documented for areas of increased fracture density.

Fracture apertures also increase across the RCF and GMF (Fig. 12). Cooling contraction of the tuff may have produced fracture apertures, but I note that many localities in the Bandelier Tuff show cooling joints having no aperture. If in fact tectonic displacement has been accommodated by the documented fractures over the RCF and GMF by incremental, vertical displacement on each fracture, then with summation of these displacements one can test the model of Gardner and House (1987) that shows downdrop on the west side of this fault zone. Figure 15 shows that fracture aperture can be well described by a cosine function of dip, that is there is a general increase in aperture with increasing fracture dip. This increase shows gently dipping fracture (<45°) having an aperture of ~0.6 cm, but more steeply dipping ones increase in aperture to an average of about 1.0 cm as dip increases to 90° (vertical). This relationship is similar to that found for fractures in Los Alamos Canyon by Wohletz (1996), and it supports the following interpetation of a trigonometric relationship between fracture dip and fracture aperture.

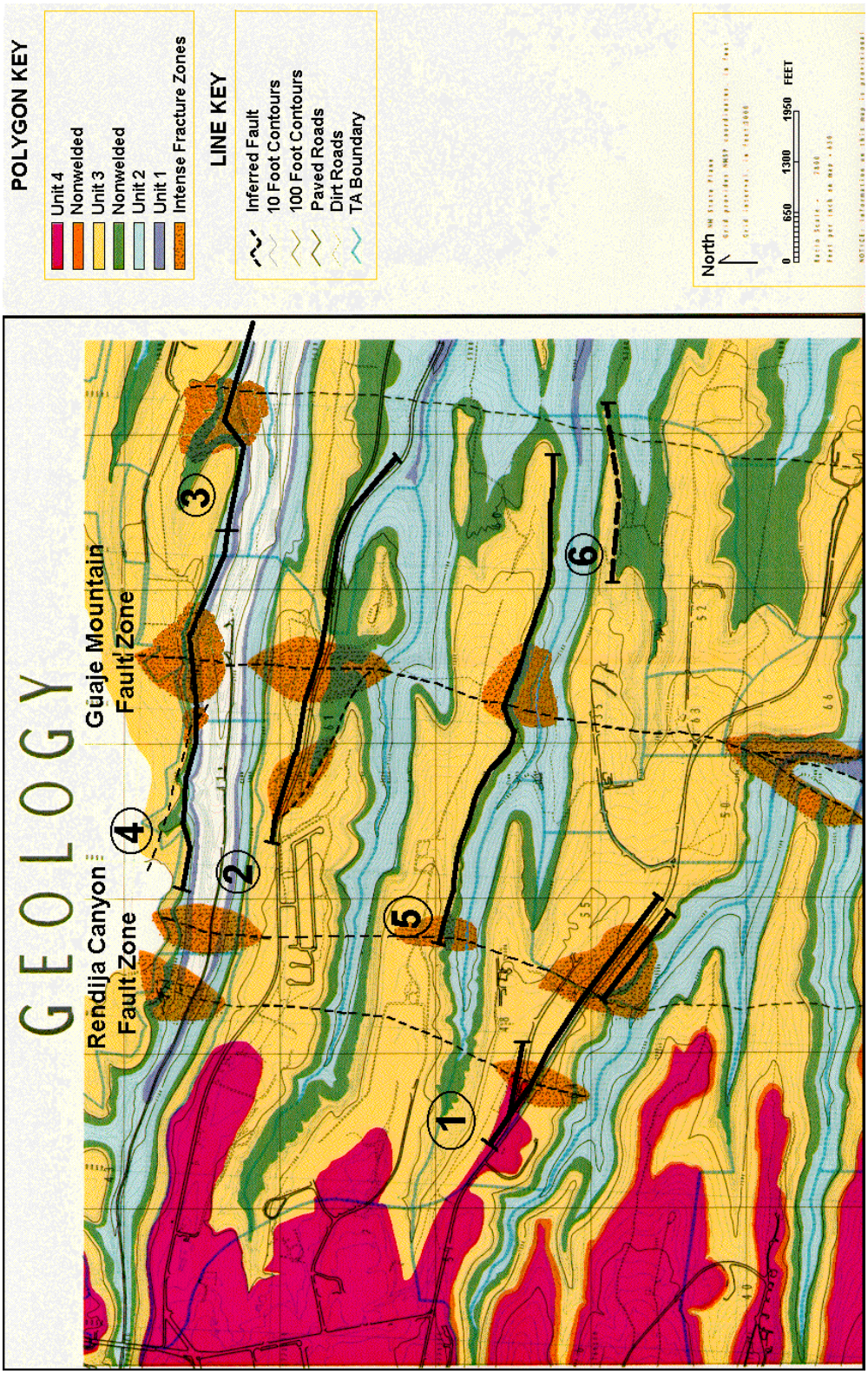

Fig. 14:Geological map of the central portion of Los Alamos National Laboratory adapted from Vaniman and Wohletz (1990), showing locations of measured sections of fracture characteristics. Section 5 along Mortandad Canyon shows newlly identified areas of intense fracturing (stippled pattern) and the prpossed trace of the Rendija Canyon Fault across Mortandad Canyon

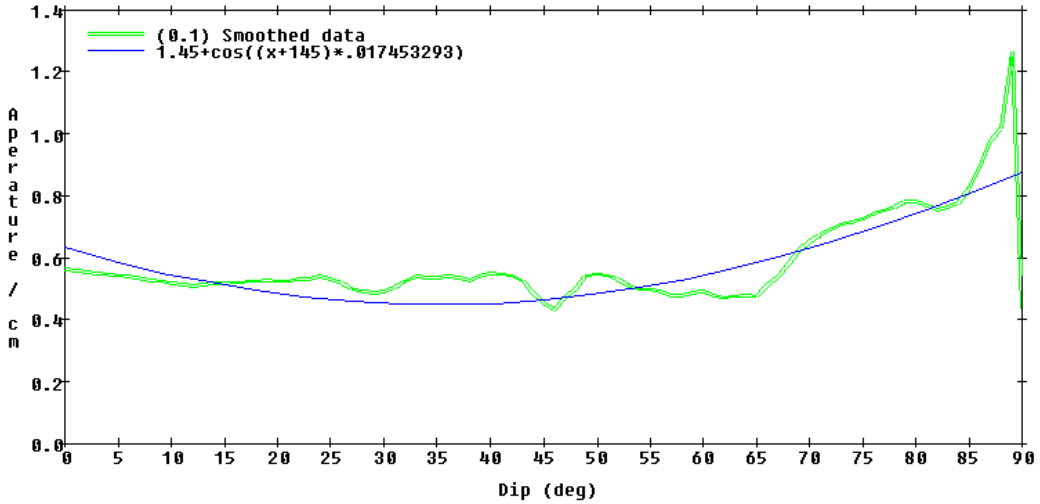

Fig. 15: Variation of fracture aperture with fracture dip showing a trigonometric fit to the smoothed data that indicates a general increase in fracture aperture with increasing dip.

Based on trigonometric arguments proposed by Wohletz (1996), one may assume that fracture apertures have developed by vertical displacement along initially closed cooling joints. This assumption supposes that fractures dipping easterly open by downdrop of the fracture foot wall, and conversely, fractures dipping westerly open by uplift of the hanging wall. This assumption is partly based on the findings of Gardner and House that there is a general downdrop to the west across the RCF and GMF. To numerically apply this assumption, I calculate the apparent vertical displacement on each fracture by dividing the aperture by the cosine of its dip, assigning positive values to this displacement where fractures dip westerly and negative values where they dip easterly. This calculation ignores E-W fractures and those that have nearly vertical or vertical dips, because their dip direction is ambiguous.

Results of this vertical displacement calculation is shown in Figures 16 as the calculated cumulative fracture displacement per 100 foot interval; the smoothed curve denotes net down drop where it is less than zero and net uplift where it is greater than zero. A pronounced zone of net down drop occurs between 400 and 1400 feet east (RCF), reaching nearly 150 cm per 100-foot interval. Another zone between 2800 and 4400 feet east shows moderate down drop with a central uplift or horst, which was found by Wohletz (1966) to be the signature of the GMF in Los Alamos Canyon. Figure 17 shows net displacement over the entire measured section. East of 5400 feet there is zero net displacement, but from 5400 feet west to 3100 feet net down drop

reaches 3.7 m, shown by a 2-m-deep graben structure between 3900 and 5300 with a small horst at 4100 to 4200 feet and a steep drop at 3100 feet of ~3.7 m. This profile again nearly matches that of the GMF in Los Alamos Canyon (Wohletz, 1996), indicating that the Bandelier Tuff deforms over the GMF similarly in both these canyons. Between 1100 and 3100 feet, there is negligible displacement, but between 500 and 1100 feet there is 11.3 m of down drop, coincident with the proposed trace of the RCF. These observations support the model of Gardner and House (1987). Because this hypothetical calculation reveals such structurally consistent results that mimic those found in Los Alamos Canyon (at least for the GMF), there must be an underlying order to the sequential progression of strike, dip, and aperture in fractures measured in Mortandad Canyon; these measurements could not give such calculated results if they were randomly distributed.

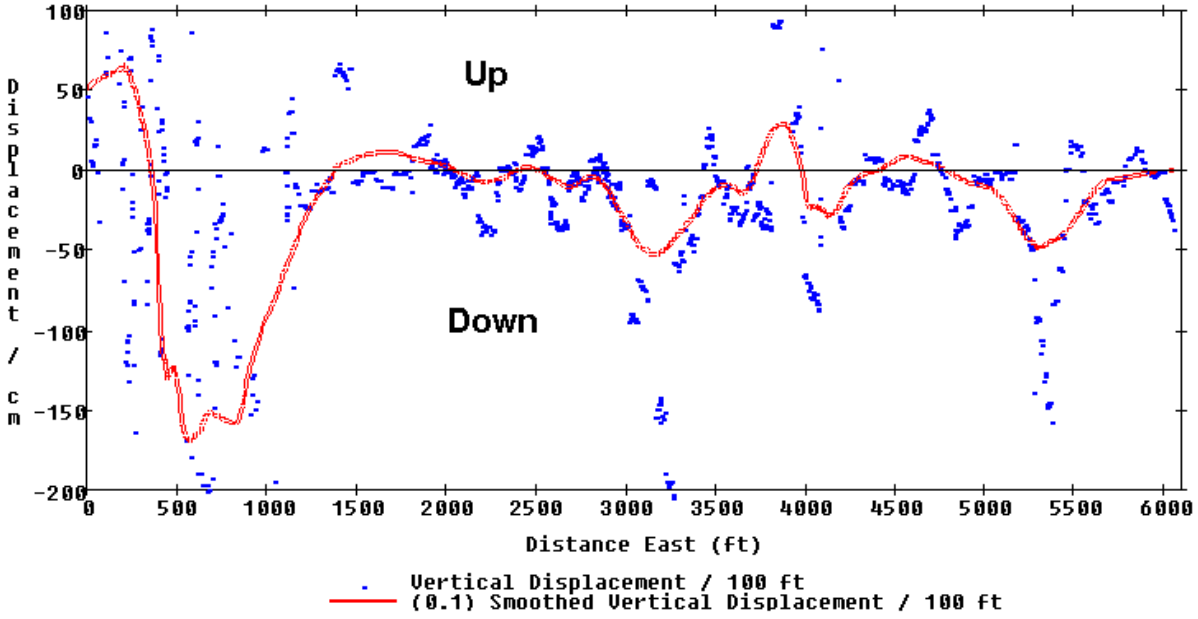

Fig 16: Variation of calculated vertical displacement in centimeters over 100-foot intervals from west to east along the measured section. A pronounced down-drop is evident between 400 and 1100 feet east, which corresponds to the trace of the Rendija Canyon Fault. Both down drops and uplifts are noted between 2800 to 5500 feet east, a reflection of the broad area affected by the Guaje Mountain Fault.

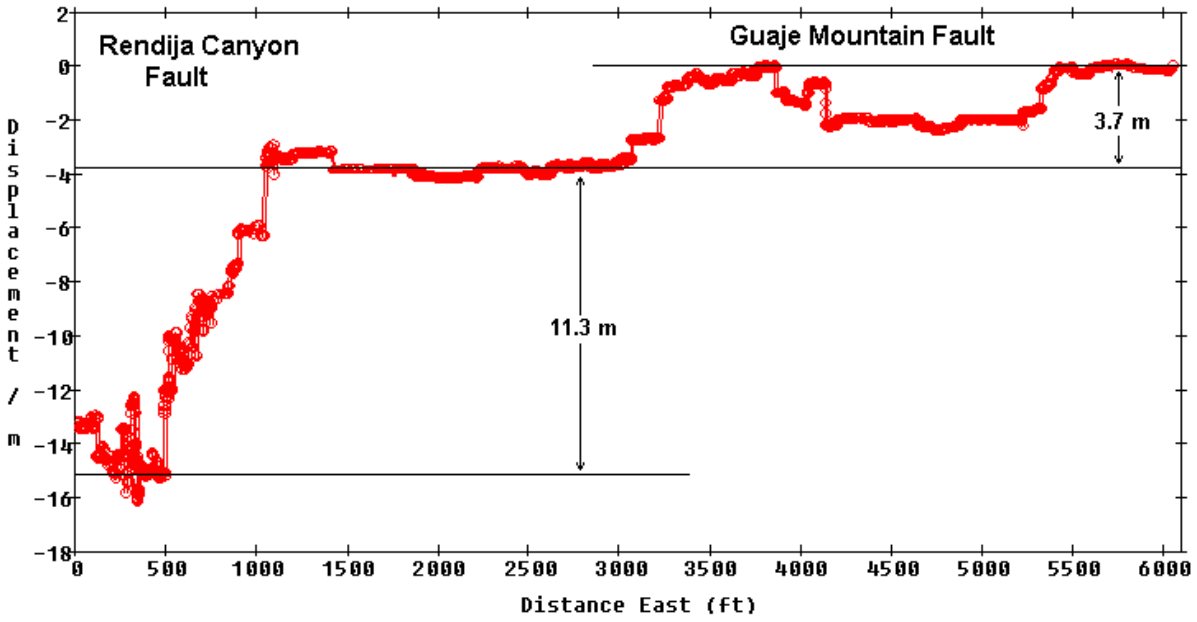

Fig 17: Cumulative calculated vertical displacement in meters along the Mortandad section, showing 11.3 m of down drop across the Rendija Canyon Fault (200 to1100 feet east) and 3.7 m of down drop across the Guaje Mountain Fault (3300 to 5400 feet east). Note Guaje Mountain Fault has a very similar profile and displacement as was calculated for it in Los Alamos Canyon in OU-1098 by Wohletz (1996).

Fracture strikes indicate the presence of a conjugate fracture set with mean trends of N22W and N82E, which is similar to published work on welded tuff (Fuller and Sharp, 1992). Wohletz (1966) suggested that a E-W fracture set might occur in Los Alamos Canyon along with observed NW and NE trends, based on a mathematical compensation for the biasing caused by measurement along a nearly E-W line. The observations presented here support that suggestion since the NE set is oriented nearly E-W. By inspection of the strike rose diagram (Fig. 6), a third more truly NE trend at N50E is only poorly developed. Both fracture strike sets and dip sets show indications of antithetic behavior across the fault zones; that is the angle between the strikes of each fracture set and that between the dip of each fracture set tends to increase. Away from faults, the angle tends to stay the same; that is where the NW-striking and N-dipping sets become more westerly in strike, the NE-striking and S-dipping fractures tend to become more northerly in strike. The reason for this behavior is unclear and requires a further study on the relationship of tectonic movement and fracture development in the tuff, a subject for future study.

Fracture Origins. The origin of conjugate joints can be attributed to cooling contraction of the tuff after its emplacement. While such an origin hypothetically produces a 60° angle between fracture sets in an isotropic medium, existence of stress anisotropy will cause deviations from the 60° angle (MacDonald, 1975). The N22W and ~N50E fracture trends indicates a principal horizontal stress field oriented approximately N15E. Anisotropy, indicated by the N82E fracture set, might have arisen if tuff cooling and compaction occurred over the shoulder of the pre-Tshirege canyon, hypothesized by mapped thickening of the tuff in canyons (Smith et al., 1970). Such compaction over canyon walls would produce a dominant N-S flexure with strain accommodated by E-W trending.

The observed steep dip on most fractures is predicted by models of the growth of cooling contraction joints (DeGraff and Aydin, 1993). Assuming the tuff to be initially homogeneous and subjected to isotropic stresses prior to during compaction, fractures should develop and propagate normal to evolving isotherms during cooling. Such a model crudely predicts the observed pattern of steeply dipping fractures. Fracture dips are dominantly to the north. This observation can be explained by the proximity of unit 2 to a possible pre-Bandelier topographic surface, which was also a north canyon wall. If fractures propagate during cooling contraction normal to isotherms and the isotherms parallel the cold substrate, then fractures would be expected to develop with a northerly dip in this region.

Hydrologic Effects. A review of tuff hydrology is given by Wood and Fernandez (1988), who compile tuff data from a variety of sources. Fuller and Sharp (1992) show that the existence of fractures in tuff strongly controls effective rock permeability. In addition, fractures in tuff have been characterized at Yucca Mountain in recognition of their role on hydraulic response (Barton and Hsieh, 1989; Barton and Larsen, 1985). One hydrological effect may be the a greater penetration depth of surface water from runoff and the canyon stream (Fuller and Sharp, 1992). If such increased penetration has occurred over time, then one might expect to find greater development of tuff alteration products (e.g., clays and zeolites) in the tuff below the canyon floor over these fault zones. This reasoning then suggests two fates for groundwater infiltration: (1) the increased fracture permeability has enhanced infiltration; and (2) development of tuff alteration materials has partly or completely sealed fractures producing a lower permeability in the region, thus decreasing infiltration. If the first is true then from the conclusions presented

above, the increased fracturing in the Bandelier Tuff across the RCF and GMF might provide infiltration for stream flow in the canyon, especially for GMF, which is just down stream from the confluence of Effluent Canyon. Such infiltration may allow contaminants carried in runoff moving down canyon to infiltrate rock below the canyon floor, perhaps reaching perched aquifers below and infiltrating an alluvial aquifer down canyon. Despite the affects of increased tuff alteration mentioned in the second fate, evidence from studies by Fuller and Sharp (1992) demonstrate that the presence of weathering (fracture coatings) on tuff surfaces decreases its surface permeability by an order of magnitude. This effect reduces the degree of water interchange between fractures and the tuff matrix and allows a high degree of deep infiltration. In support of the latter fate, fractures observed within several tens of feet from mesa tops generally contain fill materials including infiltrated detritus, gypsum, and likely clays and zeolites, which have been found to greatly retard water infiltration (Abrahams et al., 1961). But at greater depths in Tshirege Member, fractures are generally open (Vaniman and Wohletz, 1990), and they provide a large capacity for fluids (Purtymun et al., 1989).

CONCLUSIONS

In documentation and measurement of 2296 fractures in unit 3 of the Tshirege Member along Mortandad Canyon between OU-1114 and OU-1129, prominent increases in fracture density are found to exist where the RCF and GMF cross the canyon. Fracture spacing ranges from background values of ~5 feet to <1 foot over fault zones. From analysis of apparent fracture displacement, vertical movement over these faults has occurred in the measured section from 500 to 1100 feet east (RCF) and from 3300 to 5300 feet east (GMF), and the displacement is down to the west. The calculated displacement is 11.3 and 3.7 m for the RCF and GMF, respectively. This result can only have been calculated if there is some non-random progression in fracture characteristics along the measured section.

The fractures occur in two dominant sets, one with a mean strike of N22W and the other at N82E. A minor fracture set may occur near N50E. This system of fractures are conjugate in nature, having their ultimate origins from cooling contraction of the tuff with a regional principal horizontal stress oriented at ~N15E compounded by stress anisotropy produced by tuff compaction over a sloping topography of the pre-Bandelier Mortandad Canyon.

The overall conclusion of this study then suggests that water movement down Mortandad Canyon may likely be influenced where it crosses these faults. The influence, if any, would be a pathway for surface runoff infiltrated downward into bedrock, perhaps reaching a perched aquifer below and an alluvial aquifer in lower Mortandad Canyon. Most important, perhaps, is the trace of the GMF, which occurs downstream of the confluence of Effluent Canyon with Mortandad Canyon.

REFERENCES

Abrahams, J. H., Weir, J. E., and Purtymun, W. D., 1961, Distribution of moisture in soil and near-surface tuff on the Pajarito Plateau, Los Alamos County, New Mexico. U.S. Geol. Surv. Prof. Rep. No. 424-D, Washington, D.C.

Baltz, E. H., Abrahams, J. H., and Purtymun, W. D., 1963, Preliminary report on the geology and hydrology of Mortandad Canyon near Los Alamos, New Mexico, with reference to disposal of liquid low-level radioactive waste, U.S. Geol. Surv. Open File Report, Albuquerque, New Mexico.

Barton, C. C. and Hsieh, P. A., 1989, Physical and hydrologic flow properties of fractures. Int. Geol. Cong., 28th, Field trip guidebook T385, 36 pp.

Barton, C. C. and Larsen, E., 1985, Fractal geometry of two-dimensional fracture networks at Yucca Mountain, southwestern Nevada. In: Fundamentals of Rock Joints: International Symposium, Bjorkliden, Sweden, Proc. p. 77-84.

DeGraff, J. M. and Aydin, A., 1993, Effect of thermal regime on growth increment and spacing of contraction joints in basaltic lava. J. Geophys. Res., v. 98, no. B4, p. 6411-6430.

Fuller, C. M. and Sharp, J. M. Jr., 1992, Permeability and fracture patterns in extrusive volcanic rocks: Implications from the welded Santana Tuff, Trans-Pecos Texas. Geol. Soc. Amer. Bull., v. 104, p. 1485-1496.

Gardner, J. N. and House, L., 1987, Seismic hazards investigations at Los Alamos National Laboratory, 1984-1985. Los Alamos National Laboratory report LA-11072-MS, 76 pp.

MacDonald, G. A., 1975, Volcanoes, Prentice-Hall, Inc., Englewood Cliffs, NJ, 510 pp.

Purtymun, W. D. and Kennedy, W. R., 1971, Geology and hydrology of Mesita del Buey. Los Alamos Scientific Laboratory report LA-4660.

Purtymun, W. D., Wheeler, M. L., and Rogers, M., 1978, Geologic description of cores from holes P-3 MH-1 through P-3 MH-5, Area G, Technical Area 54, Los Alamos Scientific Laboratory report LA-7308-MS.

Purtymun, W. D., Enyart, E. A., and McLin, S. G., 1989, Hydrologic characteristics of the Bandelier Tuff as determined through an injection well system. Los Alamos National Laboratory Rep. No. LA-11511-MS, Los Alamos, New Mexico.

Smith, R. L., Bailey, R. A., and Ross, C. S., 1970, Geologic map of the Jemez Mountains, New Mexico. U.S. Geol. Surv. Misc. Geol. Invest. Map, I-571.

Vaniman, D. and Wohletz, K., 1990, Results of geological mapping/fracture studies: TA-55 area. Los Alamos National Laboratory Seismic Hazards Memo EES1-SH90-17, 25 pp, 3 Plates, 23 figures.

Walters, M. C., 1996, Fracture analysis of the Bandelier Tuff, Pajarito Plateau, north-central Rio Grande Rift, New Mexico, M. S. thesis, Texas Christian University, Fort Worth, Texas, 92 pp.

Wohletz, K. H., 1995, Measurement and analysis of rock fractures in the Tshirege Member of the Bandelier Tuff along Los Alamos Canyon adjacent to TA-21. In: Earth Science Investigations for Environmental Restoration—Los Alamos National Laboratory Technical Area 21 (DE Broxton and PG Eller, eds.), Los Alamos National Laboratory report LA-12934-MS, 19-31.

Wohletz, K. H., 1996, Fracture characterization of the Bandelier Tuff in OU-1098 (TA-2 and TA-41), Los Alamos National Laboratory Report LA-13194-MS, 19 pp.

Wood, W. W. and Fernandez, L. A., 1988, Volcanic rocks. in The Geology of North America, Volume O-2, Hydrogeology, Boulder, Colorado, Geol. Soc. of Amer., p. 353-365.